Stimulated Terahertz Emission from Intraexcitonic Transitions in Cu_2O

Rupert Huber,* Ben A. Schmid, Y. Ron Shen, Daniel S. Chemla, and Robert A. Kaindl

Department of Physics, University of California at Berkeley, and Materials Sciences Division, E.O. Lawrence Berkeley National Laboratory, Berkeley, California 94720, USA

(Received 12 June 2005; published 6 January 2006)

We report the first observation of stimulated emission of terahertz radiation from internal transitions of excitons. The far-infrared electromagnetic response of Cu_2O is monitored via broadband terahertz pulses after ultrafast resonant excitation of three-dimensional $3p$ excitons. Stimulated emission from the $3p$ to the energetically lower $2s$ bound level occurs at a photon energy of 6.6 meV, with a cross section of $\sim 10^{-14}$ cm^2. Simultaneous excitation of both exciton levels, in turn, drives quantum beats, which lead to efficient terahertz emission sharply peaked at the difference frequency.

DOI: 10.1103/PhysRevLett.96.017402 PACS numbers: 78.45.+h, 42.65.−k, 71.35.−y, 78.47.+p

Excitons, Coulomb-bound pairs of one electron and one hole, are often seen as the low-energy counterpart of the hydrogen atom. This picture has been successfully invoked to describe photoexcitation of a semiconductor in the low-density limit [1,2]. The analogy to atoms has also motivated the search for macroscopically ordered states and Bose-Einstein condensation of excitons in two-dimensional nanostructures [3] or bulk cuprous oxide (Cu_2O) [4,5]. Nevertheless, there are significant limitations to the atomiclike description of excitons. These quasiparticles are complex many-body states embedded in the background of a crystal lattice, which interact via scattering, phase-space filling, and screening. They generally exist in a mixture with unbound charge carriers. Unlike atoms, excitons are transiently photogenerated, associated with an initial interband coherence, and subject to decay by recombination. Testing the concept of excitons has thus been an important focus in semiconductor physics [6].

Most of the spectroscopic information has been extracted from optical techniques probing interband transitions. However, such experiments provide only indirect access to the internal exciton structure. A most direct approach is to investigate intraexcitonic absorption resonantly in the mid- to far-infrared spectral domain [5,7,8]. In recent years, various sources for terahertz (THz) radiation have been developed [9]. THz spectroscopy has evolved as a powerful tool for probing low-energy excitations in semiconductors with ultrafast temporal resolution [7,10,11]. Recently, absorption of THz photons promoting ground state excitons into higher bound energy levels was used to explore exciton formation [7].

Theoretical studies suggest how the underlying elementary quantum processes could be effectively reversed to induce THz gain from inverted exciton populations [12,13]. However, scattering with phonons, excitons, and free carriers leads to ultrafast nonradiative relaxation of the excited states to the lowest bound exciton level. These processes and THz absorption into higher bound and continuum states can strongly compete with stimulated emission and are poorly understood. Up to now, stimulated emission of THz radiation connecting internal exciton levels has not been observed.

In this Letter, we present the first direct observation of stimulated emission of electromagnetic radiation from intraexcitonic transitions. After resonant photoexcitation of $3p$ excitons in the semiconductor Cu_2O we use broadband THz pulses to induce internal dipole transitions to the $2s$ state. This process manifests itself via a negative change of the absorption coefficient at the resonant photon energy of 6.6 meV. Ultrafast dynamics, linewidths, positions, and oscillator strengths of this and other internal exciton transitions are directly mapped out. Furthermore, we observe unexpected efficient THz emission at 6.6 meV when the visible pump pulse covers both dipole-active $3p$ and optically dark $2s$ states.

All experiments are performed at low temperature ($T = 6$ K) in a 330 μm thick, naturally grown high-quality Cu_2O crystal. The visible absorption spectrum (Fig. 1) is dominated by a series of sharp lines originating from the $2p$, $3p$, $4p$, and $5p$ excitons (yellow series), followed by the continuum of unbound states. Owing to the positive parity of the valence and conduction band minima at the Brillouin zone center, even parity s and d excitons are dipole forbidden [14]. Figure 1 shows a detailed exciton term scheme, with the energy difference to the $3p$ level given on the left. Far-infrared transmission measurements confirm the unexcited sample to be transparent with no absorption features in the window between 1 and 12 meV.

Our experimental scheme is based on an ultrafast regenerative Ti:sapphire amplifier operating at 250 kHz repetition rate, which delivers 42 fs light pulses at a center wavelength of 800 nm. Near-bandwidth-limited light pulses tunable around 575 nm wavelength are obtained by subsequent optical parametric amplification. We use a grating-based pulse shaper to tailor the energy and width of these visible pulses, in order to selectively photoexcite specific bound exciton states or the continuum of unbound electron-hole (e-h) pairs. A resulting typical pump spectrum is indicated by the dashed curve in Fig. 1. Ultrashort THz probe pulses are obtained by difference frequency mixing within the broad spectrum of a second branch of

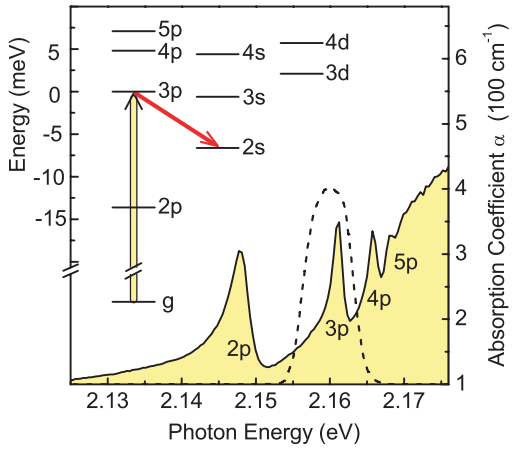

FIG. 1 (color online). Optical absorption spectrum of the Cu_2O crystal studied in this work, at $T = 6$ K. Exciton absorption lines exhibit widths of 3.6 meV ($2p$) and 1.8 meV ($3p$). The term scheme indicates the yellow exciton series, with energy differences given with respect to the $3p$ exciton level [14]. Resonant excitation of $3p$ excitons is indicated by the thick upward arrow (a corresponding typical pump spectrum is shown by the dashed curve). Internal exciton transitions from p to s or d states are dipole allowed (solid arrow).

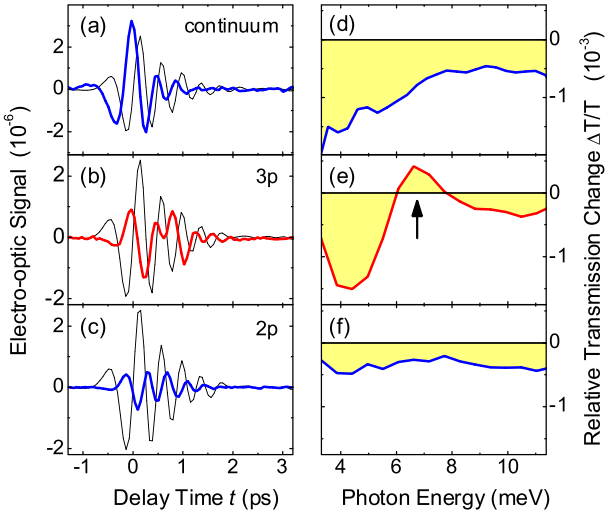

FIG. 2 (color online). (a)–(c) Pump-induced changes ΔE_{THz} (thick lines) at $\Delta t = 1$ ps after excitation, and reference THz fields E_{THz} (thin lines, downscaled by a factor of 500) without excitation. Pump spectra are centered (a) in the continuum at 2.206 eV, (b) at the yellow $3p$ exciton line, and (c) at the $2p$ exciton line. (d)–(f) Corresponding relative transmission changes $\Delta T/T$. Arrow: enhanced transmission at 6.6 meV.

the near-infrared laser output. This process of optical rectification is achieved in a 500 μm thick ZnTe crystal exploiting its large second order nonlinearity $\chi^{(2)}$ [9]. The real-time electric field trace $E_{\mathrm{THz}}(t)$ of the transmitted THz pulse is recorded by means of electro-optic sampling with a large signal-to-noise ratio of 10^5. Measurement of the THz field directly in the time domain yields both real and imaginary parts of the optical response on equal footing.

In a first set of experiments, we resonantly excite the Cu_2O sample at specific exciton absorption lines and follow the subsequent transient changes in the far-infrared response via a time-delayed THz pulse. Figures 2(a)–2(c) show the transmitted THz field $E_{\mathrm{THz}}(t)$ without photoexcitation (thin lines, downscaled by a factor of 500), and its transient change $\Delta E_{\mathrm{THz}}(\Delta t, t)$ (thick lines) induced by photoexcitation at three characteristic wavelengths. The temporal delay between the yellow pump pulse and the electro-optic gating pulse is kept fixed at $\Delta t = 1$ ps. Differential transmission spectra $\Delta T/T$ corresponding to each case are shown in the right panels of Fig. 2. The response reveals a critical wavelength dependence: excitation in the continuum [Figs. 2(a) and 2(d)] or at the $2p$ resonance [Figs. 2(c) and 2(f)] induces electric field transients that resemble the reference pulse with a phase offset. A featureless broadband decrease of transmission results. In contrast, resonant excitation of $3p$ excitons shows a very different shape of the induced field and a strongly structured transmission change [Figs. 2(b) and 2(e)]. In particular, we find a remarkable increased transmission around 6.6 meV photon energy.

Knowing the THz electric fields in both amplitude and phase, we directly determine the change of the complex refractive index $\tilde{n}(\omega) \equiv n(\omega) + i\frac{c}{2\omega}\alpha(\omega)$, where n denotes the real part of the refractive index and α the absorption coefficient. Since the excitation density decays exponentially along the propagation length z inside the crystal, we express the locally induced change as $\Delta\tilde{n}(z, \omega) = \Delta\tilde{n}(\omega)\exp\{-\alpha_{\mathrm{vis}}z\}$. Here, α_{vis} is the absorption coefficient in the visible (Fig. 1) and $\Delta\tilde{n}(\omega)$ refers to the pump-induced change at the entrance face of the crystal. Based on this and including the refractive index of Cu_2O [15], the complex transfer function of the photoexcited sample is calculated via the Fresnel matrix formalism. In turn, we directly obtain the induced change of refractive index and absorption at each frequency by solving for $\Delta\tilde{n}(\omega)$ to match the resulting response function with the experimental data.

Figure 3 displays the differential changes Δn and $\Delta\alpha$ obtained from the traces in Fig. 2. Continuum excitation [topmost curves in Figs. 3(a) and 3(b)] results in a predominantly inductive THz response, well explained by the Drude theory (dash-dotted lines) of a conducting e-h gas. In contrast, resonant $2p$ excitation induces only small changes in the refractive index (lowest curves in Fig. 3) as expected for insulating, bound states. The most striking response is obtained after selective excitation of the $3p$ interband resonance, yielding a pronounced spectral structure in both $\Delta\alpha$ and Δn. With increasing frequency, a peak of enhanced absorption occurs at 4.5 meV, followed by a narrow minimum of $\Delta\alpha$ at 6.6 meV. Indeed, here the induced absorption becomes negative. We emphasize three key aspects of this observation: (i) unexcited Cu_2O shows no discernible THz absorption in this frequency range, (ii) the minimum with $\Delta\alpha < 0$ appears exclusively after

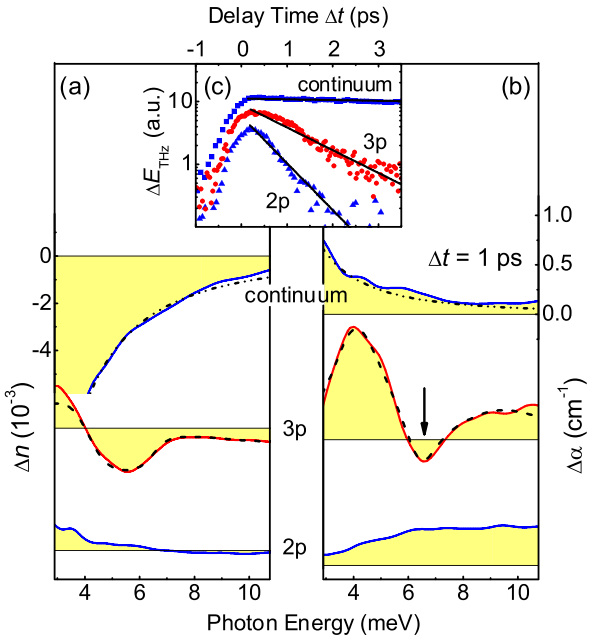

FIG. 3 (color online). THz response at $\Delta t = 1$ ps after excitation of $2p$ or $3p$ excitons, or the continuum. (a),(b) Changes of refractive index Δn and absorption $\Delta\alpha$ (solid lines, offset vertically for clarity). Dash-dotted lines: a Drude response (topmost curves) with screened plasmon energy $\hbar\omega_{\mathrm{pl}} = 0.3$ meV and damping $\Gamma/2\pi = 0.4$ meV. Dashed lines: model of three oscillators (lower curves) with energies (and linewidths) $E_1 = 4.5$ meV (2.5 meV), $E_2 = 6.6$ meV (1.6 meV), and $E_3 = 9.5$ meV (4 meV), and relative oscillator strengths as given in the text. The vertical arrow marks the negative absorption change occurring around 6.6 meV. (c) Ultrafast pump-probe dynamics of the induced change of the THz field at corresponding pump energies.

resonant excitation of $3p$ excitons, and (iii) the observed resonance energy of 6.6 meV is precisely identical with the $3p$-$2s$ level spacing (Fig. 1). Hence, we can identify the negative absorption peak as stimulated emission of THz radiation via the $3p \rightarrow 2s$ intraexcitonic transition.

For further analysis, we model the line shape of the THz response upon $3p$ excitation. A faithful representation of the experiment is achieved with a model of three oscillators (dashed lines, Fig. 3). Referring to the term scheme of Fig. 1, we attribute the lowest-frequency oscillator centered at 4.5 meV to the joint effects of $3p \rightarrow 4s$ and $3p \rightarrow 4d$ transitions. The center oscillator at 6.6 meV exhibits a negative oscillator strength, in accordance with the $3p \rightarrow 2s$ stimulated emission. Finally, a component at 9.5 meV phenomenologically describes all transitions to higher bound states. The relative oscillator strengths $f_1{:}f_2{:}f_3 = 2.7{:}(-1){:}1.1$ agree qualitatively with a hydrogen model [4.4:(−1):2], thus supporting this assignment [16]. A more rigorous theory should also take into account the partial d character of the $2s$ exciton in Cu_2O, as described in Ref. [14]. With an estimated density of $3p$ excitons of 3×10^{13} cm^{-3} we obtain a cross section for the $3p \rightarrow 2s$ transition of $\sigma \approx 10^{-14}$ cm^2. This value compares well with order-of-magnitude estimates based on hydrogenic exciton wave functions [12]. Since the excitation densities reached in our setup are several orders of magnitude below the excitonic Mott density, higher pump energies make this approach potentially interesting for efficient THz amplification.

It should be noted that the THz emission may be sensitive to two types of excitations [13,17]: (i) *Coherent excitonic polarizations,* where THz emission results from stimulated Raman scattering as a single-step nonlinear optical process: the THz field coherently couples polarizations from the $3p$ to the $2s$ state, from which in turn visible pump photons are scattered into the THz field. (ii) *Exciton populations,* where stimulated emission is driven purely by population inversion and subsequent hot luminescence, analogous to atomic lasers. The relative importance of these processes depends on the polarization and population decay times. A dephasing time for the $3p$ level can be estimated from the visible linewidth, which yields $T_2 \approx 0.7$ ps assuming predominantly homogeneous broadening for our high-quality Cu_2O crystal. Population relaxation can be deduced from the dynamics of the induced THz response. Figure 3(c) depicts an increasingly faster exponential decay as we turn from continuum states ($\tau = 36$ ps), via the $3p$ ($\tau = 1.3$ ps) to the $2p$ exciton ($\tau = 0.8$ ps). The relative spectral shape does not vary strongly within the respective decay time (not shown). The relaxation is explained by recombination and scattering into $1s$ excitons mediated by optical phonon interactions [18]. On this basis, stimulated THz emission after $3p$ excitation occurs both during an initial regime of coherent excitonic polarizations and from the subsequent incoherent regime of inverted population.

In the following, we show that coherent manipulation of the $3p \rightarrow 2s$ transition may be exploited to emit THz radiation even without stimulation by external THz fields. For this second set of experiments, the pump spectrum is tuned to simultaneously overlap both the $3p$ and the dipole-forbidden $2s$ resonances. No THz probe light is incident on the sample. We observe emission of a coherent THz field. The transient [Fig. 4(a)] is detected electro-optically by scanning the delay Δt between the visible pump and the near-infrared gating pulse. The corresponding power spectrum in Fig. 4(b) peaks at 6.6 meV and exhibits a width of 1.7 meV (FWHM). This line shape coincides with the values deduced from the $3p \rightarrow 2s$ transition in Fig. 3, corroborating that the THz transient originates from the same internal exciton transition. The absolute size of these emitted fields is comparable to the transients ΔE_{THz} in Fig. 2 stimulated by a far-infrared seed pulse. This fact implies that the generation mechanism cannot be explained by a spontaneous version of the emission process discussed above. Moreover, we find that the THz polarization is parallel to the linear polarization of the pump light. In contrast, the polarization of the stimulated change ΔE_{THz}, described further above, is determined by the probe pulses.

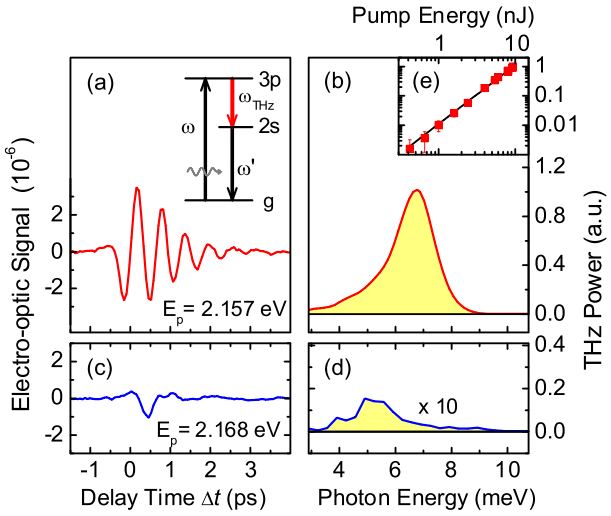

FIG. 4 (color online). THz generation in Cu_2O: (a) Real-time trace and (b) normalized power spectrum of THz pulses (FWHM: 1.7 meV) obtained with the pump centered at 2.157 eV (close to the $3p$ resonance). The spectral width of the pump pulse is 12 meV (FWHM). Inset: term scheme of the underlying quantum process. (c),(d) THz emission for pump centered at 2.168 eV. (e) The emitted THz power for excitation at 2.157 eV scales quadratically as a function of the pump pulse energy.

We interpret this THz emission as resulting from quantum beats between coherent exciton polarizations. Visible light induces $3p$ exciton polarizations, while the low-energy wing of the pump spectrum couples the $2s$ level to the ground state, e.g., via a weak quadrupole or surface field assisted dipole transition [12,19]. As $3p$ and $2s$ states feature opposite parity, quantum beats between them act as a radiating dipole. The THz generation may be expressed as an effective difference frequency process, described by the nonlinear susceptibility [20]

$$\chi^{(2)}_{\mathrm{eff}} \propto \frac{M_{3p} M_{2s} M_{3p\text{-}2s}}{(\omega - \omega_{3p} + i\Gamma_{3p})(\omega_{\mathrm{THz}} - \omega_{3p\text{-}2s} + i\Gamma_{3p\text{-}2s})},$$

where M_{3p} and M_{2s} are the visible interband matrix elements and $M_{3p\text{-}2s}$ is the THz dipole matrix element. Furthermore, ω and ω_{THz} are the frequencies of visible pump and emitted THz fields, and ω_{3p} and $\omega_{3p\text{-}2s}$ are visible $3p$ and THz $3p \rightarrow 2s$ resonance energies with corresponding dephasing constants Γ_i. The three-wave interaction is schematically indicated in Fig. 4(a). In our experiment both terms in the denominator become resonant, which leads to a high nonlinearity despite the relative weakness of the coupling between $2s$ excitons and the ground state. Off-resonant pumping reduces the conversion efficiency dramatically [Figs. 4(c) and 4(d)]. As shown in Fig. 4(e), the emitted THz intensity scales quadratically with the pump power, which further supports this $\chi^{(2)}$ picture. From the pulse intensities and effective interaction length we estimate a nonlinearity of $\chi^{(2)}_{\mathrm{eff}} \gtrsim 10$ pm/V. This value exceeds the high background nonlinearity of non-centrosymmetric materials such as ZnTe, which is widely used for THz generation [21].

In conclusion, we report the first observation of stimulated emission of far-infrared radiation from internal transitions in excitons. Broadband THz spectroscopy directly maps out the ultrafast dynamics, spectral positions, widths, and oscillator strengths of intraexcitonic transitions in Cu_2O. Stimulated emission occurs at 6.6 meV after resonant excitation of $3p$ excitons. The picture is further corroborated by the independent observation of strong THz emission at this energy due to $2s$-$3p$ quantum beats. Our results provide a new, fundamental test of excitonic quantum physics, and highlight differences and analogies to atomic systems.

We thank N. C. Nielsen for valuable discussions. This work was supported by the Office of Science, Office of Basic Energy Sciences of the U.S. Department of Energy under Contract No. DE-AC03-76SF00098. R. H. acknowledges support from the Alexander von Humboldt Foundation.

*Corresponding author.
Electronic address: rhuber@lbl.gov

[1] E. I. Rashba, *Excitons* (North-Holland, Amsterdam, 1982).
[2] H. Haug and S. W. Koch, *Quantum Theory of the Optical and Electronic Properties of Semiconductors* (World Scientific, Singapore, 2004).
[3] L. V. Butov *et al.*, Nature (London) **417**, 47 (2002).
[4] D. W. Snoke *et al.*, Phys. Rev. Lett. **64**, 2543 (1990); K. E. O'Hara and J. P. Wolfe, Phys. Rev. B **62**, 12 909 (2000).
[5] M. Kubouchi *et al.*, Phys. Rev. Lett. **94**, 016403 (2005).
[6] For a review see, e.g., D. S. Chemla and J. Shah, Nature (London) **411**, 549 (2001), and references therein.
[7] R. A. Kaindl *et al.*, Nature (London) **423**, 734 (2003).
[8] M. Jörger *et al.*, Phys. Status Solidi B **238**, 470 (2003).
[9] For a review see, e.g., B. Ferguson and X.-C. Zhang, Nat. Mater. **1**, 26 (2002), and references therein.
[10] R. Huber *et al.*, Nature (London) **414**, 286 (2001); R. Huber *et al.*, Phys. Rev. Lett. **94**, 027401 (2005).
[11] C. W. Luo *et al.*, Phys. Rev. Lett. **92**, 047402 (2004).
[12] S. Nikitine, J. Phys. Chem. Solids **45**, 949 (1984).
[13] M. Kira and S. W. Koch, Phys. Rev. Lett. **93**, 076402 (2004).
[14] C. Uihlein *et al.*, Phys. Rev. B **23**, 2731 (1981).
[15] *Cuprous Oxide (Cu_2O) Optical Properties*, Landoldt-Börnstein, Group III Condensed Matter, Subvolume C (Springer, Berlin, 1998).
[16] H. A. Bethe and E. E. Salpeter, *Quantum Mechanics of One- and Two-Electron Atoms* (Academic Press, New York, 1957).
[17] Y. R. Shen, Phys. Rev. B **14**, 1772 (1976).
[18] P. Y. Yu and Y. R. Shen, Phys. Rev. B **17**, 4017 (1978).
[19] S. Lien Chuang *et al.*, Phys. Rev. Lett. **68**, 102 (1992).
[20] The relation follows from a simplified treatment of stimulated polariton scattering as discussed in Y. R. Shen, *The Principles of Nonlinear Optics* (Wiley, New York, 2002).
[21] Q. Wu and X.-C. Zhang, Appl. Phys. Lett. **68**, 1604 (1996).